Int. J. Heat Mass Transfer. Vol. 33, No. 12, pp. 2599–2608, 1990
Printed in Great Britain

0017–9310/90 $3.00 + 0.00

Second-order corrections of the k–ε model to account for non-isotropic effects due to buoyancy

LARS DAVIDSON†
Department of Applied Thermodynamics and Fluid Mechanics, Chalmers University of Technology, S-412 96 Gothenburg, Sweden

(*Received* 30 *October* 1989 *and in final form* 13 *January* 1990)

Abstract—A new turbulence model which is a hybrid of the k–ε model and an algebraic Reynolds stress model (ASM) is developed. This model takes from an ASM that part of the non-isotropic Reynolds stress which is due to buoyancy, and the remaining part from the k–ε model. This concept is also applicable to flows with rotation where the Coriolis forces affect the turbulence by increasing its non-isotropy. The model is tested in a buoyancy-driven cavity flow. The contributions from the ASM corrections to the Reynolds stress and the turbulent heat flux are up to five and ten times, respectively, larger than those from the k–ε model.

1. INTRODUCTION

TWO-EQUATION turbulence models, such as the k–ε model, have been used for many years by researchers, and are still being used extensively. Today numerical simulation using the k–ε model is also becoming an important tool for engineers in industry. The model, despite its simplicity, produces fairly accurate results for a wide range of applications, and it is computationally rather cheap (two extra partial differential equations are solved). It is, furthermore, very robust and the turbulence model itself seldom leads to convergence problems. One important deficiency is the assumption of isotropy of the turbulence, insofar as all normal Reynolds stresses are assumed to be equal (at least in two-dimensional configurations). As a consequence, the model cannot account for buoyancy effects, for which, in stable stratified flows, the vertical fluctuating turbulent velocity is damped, and the horizontal ones are amplified [1].

Reynolds stress models, in which a *partial differential* equation is solved for each Reynolds stress, do account for these buoyancy effects; this is also the case for the algebraic Reynolds stress models, in which an *algebraic* equation is solved for each Reynolds stress [2, 3]. Both of these types of models (especially the former) are computationally much more expensive than the k–ε model, and they are, numerically, also very unstable which can lead to serious convergence problems [4, 5].

In the present work a new turbulence model which is a hybrid of the k–ε model and the algebraic Reynolds stress model (ASM) has been developed. ASM corrections are added to the Reynolds stress tensor (taken from the k–ε model) in a linear uncoupled manner. This model takes buoyancy effects into account by—in stable, stratified flows—damping vertical fluctuations and amplifying the horizontal ones, and vice versa in unstable flows.

The advantages of this hybrid model are that:

(i) it accounts for non-isotropic effects on the turbulence due to buoyancy in the same way as Reynolds stress models (which the k–ε model cannot handle); and

(ii) it is expected to be numerically much more stable than the Reynolds stress models and, thus, to decrease the computational effort for a convergent solution (or even *enable* convergence).

The test case is the buoyancy-driven flow in a tall two-dimensional cavity of 5 : 1 aspect ratio. The predicted results are compared with experimental data from Cheesewright *et al.* [6, 7], who made laser Doppler measurements in an air cavity with a Rayleigh number of 4×10^{10}. The CELS solver (Coupled Equation Line Solver), which was developed and applied to buoyancy-driven flows by Galpin and Raithby [8] and extended by the author [9], is used.

A correct treatment of the flow near the vertical walls is essential due to the large velocity gradients and the strong viscous effects prevailing there. This means that conventional wall functions, which are based on the use of local equilibrium logarithmic velocity and temperature assumptions, are not applicable. A low Reynolds number turbulence model, which can handle the strong viscous effects in the viscous sublayers near the walls, is therefore used.

This concept of modelling one part of the Reynolds stress—which is especially non-isotropic due to a particular physical phenomenon—in the same way as in an algebraic Reynolds stress model, and modelling

† Present address: CERFACS, 42 Avenue G. Coriolis, F-31057 Toulouse, France.

NOMENCLATURE

$c_1, c_2, c_3, c_\mu, c_{1\varepsilon}, c_{2\varepsilon}, c_\theta$ constants in the turbulence model
f_1, f_2, f_μ damping functions in the turbulence model
G buoyancy source term in the turbulence models
g acceleration due to gravity
g_i acceleration due to gravity in the x_i-direction
H height of cavity
k turbulent kinetic energy
L length of cavity
n coordinate in the normal direction from the wall
p pressure
P turbulence generating source term in the k and ε equations
q local heat transfer rate at the vertical walls per unit area [kW m^{-2}]
R_{ij} Coriolis production of $\overline{u_i u_j}$ (see equation (8))
R_n local Reynolds number, $\sqrt{k}n/\nu$
R_t local Reynolds number, $k^2/(\nu\varepsilon)$
t temperature [°C]
U, V mean velocity in the x- and y-directions, respectively
u, v, w turbulent fluctuation velocity in the x-, y- and z-directions, respectively
U_i mean velocity in the x_i-direction
u_i turbulent fluctuation velocity in the x_i-direction
u_* friction velocity
x horizontal Cartesian coordinate (see Fig. 1)
x^+ non-dimensional distance from the wall, xu_*/ν
x_1 x
x_2 y
x_i Cartesian coordinate in the i-direction
y vertical Cartesian coordinate (see Fig. 1).

Greek symbols
α contraction factor for the grid (see equation (9))
β coefficient of thermal expansion
δ_{ij} Kroenecker's delta
ε dissipation of turbulent kinetic energy
ε_{ijk} permutation tensor
θ turbulent fluctuating temperature
$\mu, \mu_t, \mu_{\text{eff}}$ dynamic viscosity (laminar, turbulent and effective, respectively)
ν kinematic viscosity
ρ density
σ_l laminar Prandtl number
$\sigma_k, \sigma_t, \sigma_\varepsilon$ turbulent Prandtl number for k, t and ε, respectively
τ time
$\Delta\tau$ time step
Φ general mean variable
ϕ turbulent fluctuations of general variable
Ω_p components of rotation of coordinate system (see equation (8)).

Subscripts
C cold wall
H hot wall
max maximum
ref reference value for the cavity.

the remaining part using the standard Boussinesq assumption, is also applicable to other types of flow. One example is flows where the turbulence is affected by Coriolis forces due to rotation (see Section 4.1).

In Section 2 the mean flow equations are given, and the low Reynolds number k–ε turbulence model is presented in Section 3. In Section 4 the second-order corrections of the k–ε model are derived. Results are presented and discussed in Section 5, and conclusions are drawn in Section 6.

2. THE MEAN FLOW EQUATIONS

The continuity, the momentum and the temperature equations can be written, using tensor notation, as

$$\frac{\partial \rho}{\partial \tau} + \frac{\partial}{\partial x_i}(\rho U_i) = 0 \tag{1a}$$

$$\frac{\partial}{\partial \tau}(\rho U_i) + \frac{\partial}{\partial x_j}(\rho U_i U_j) = -\frac{\partial p}{\partial x_i} + \frac{\partial}{\partial x_j}\left(\mu \frac{\partial U_i}{\partial x_j} - \rho\overline{u_i u_j}\right) + \rho g_i \tag{1b}$$

$$\frac{\partial}{\partial \tau}(\rho t) + \frac{\partial}{\partial x_i}(\rho U_i t) = \frac{\partial}{\partial x_i}\left(\frac{\mu}{\sigma_t}\frac{\partial t}{\partial x_i} - \rho\overline{u_i\theta}\right) \tag{1c}$$

where $x_1 = x, x_2 = y$ (see Fig. 1), $g_1 = 0$ and $g_2 = -g$. The density is calculated from the gas law, and the viscosity is calculated from Sutherland's formula

$$\mu = \frac{1.458 \times 10^{-6}(t+273)^{1.5}}{t+383.4}. \tag{1d}$$

Although only the steady solutions of equation (1) are of interest in this study, the equations are given in transient form, and the time step, Δt, is used as a free parameter by which the convergence rate may be

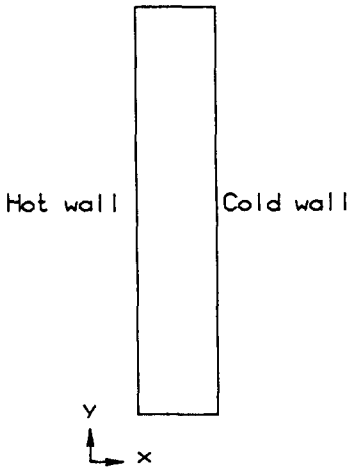

FIG. 1. Configuration. $t_C = 80°C$, $t_H = 34.2°C$, $H = 2.5$ m, $L = 0.5$ m. Vertical walls are isothermal, and horizontal walls are adiabatic.

optimized. These equations are solved using the CELS method, combined with Newton–Raphson linearization of the convective terms in the temperature equation [8]; this linearization results in a temperature-to-velocity coupling which is lost when standard linearization methods are used.

The CELS method is described in detail in the works by Raithby's group [8, 10, 11]. This solver was extended by Davidson [9] where it was used in the same configuration as here (see Fig. 1). In ref. [9] the CELS solver was found to be very efficient and robust compared with SIMPLEC of Van Doormaal and Raithby [12].

Whereas in standard iterative solvers (such as SIMPLEC) the equations are solved *sequentially*, CELS solves the *linearized* U, V, p and t equations *exactly* along a *line* estimating the off-line values with 'old' values. The domain is swept line-by-line in both directions (=one sweep) until either the residuals have been reduced to a prescribed level or a maximum number of sweeps (typically five) has been carried out; the k and ε equations are thereafter solved, and the whole cycle is repeated until convergence is reached.

The QUICK scheme by Leonard [13] was used when discretizing the convective terms. The exact form of the resulting coefficients in the discretized equations for a non-uniform grid are given in Davidson [14].

3. THE LOW REYNOLDS NUMBER k–ε MODELS

The buoyancy-driven flow in a rectangular cavity (see Fig. 1) is numerically simulated in the present work. As the flow near the walls is very important here, a low Reynolds number turbulence model, which can handle the strong viscous effects in the viscous sublayers near the walls, is used. The model by Davidson [9] can be written as

$$\frac{\partial}{\partial\tau}(\rho k)+\frac{\partial}{\partial x_i}(\rho U_i k)=\frac{\partial}{\partial x_i}\left[\left(\mu+\frac{\mu_t}{\sigma_k}\right)\frac{\partial k}{\partial x_i}\right]+\rho(P+G-\varepsilon) \quad (2a)$$

$$\frac{\partial}{\partial\tau}(\rho\varepsilon)+\frac{\partial}{\partial x_i}(\rho U_i\varepsilon)=\frac{\partial}{\partial x_i}\left[\left(\mu+\frac{\mu_t}{\sigma_\varepsilon}\right)\frac{\partial\varepsilon}{\partial x_i}\right]+\rho\frac{\varepsilon}{k}(f_1 c_{1\varepsilon}P+c_{1\varepsilon}G-f_2 c_{2\varepsilon}\varepsilon) \quad (2b)$$

where

$$x_1 = x, x_2 = y$$

$$P = -\overline{u_i u_j}\frac{\partial U_i}{\partial x_j}$$

$$\overline{u_i u_j} = -\nu_t\left(\frac{\partial U_i}{\partial x_j}+\frac{\partial U_j}{\partial x_i}\right)+\frac{2}{3}k\delta_{ij}$$

$$G = \beta g\overline{v\theta}$$

$$\overline{v\theta} = -\frac{\nu_t}{\sigma_t}\frac{\partial t}{\partial y}$$

$$\nu_t = \frac{f_\mu c_\mu k^2}{\varepsilon}, \quad \sigma_k = 1.0, \quad \sigma_\varepsilon = 1.3, \quad \sigma_t = 0.9,$$

$$c_\mu = 0.09, \quad c_{1\varepsilon} = 1.44, \quad c_{2\varepsilon} = 1.92.$$

The damping functions and the boundary conditions used are [9]

$$f_\mu = \exp\left[-\frac{3.4}{(1+R_t/50)^2}\right], \quad f_1 = 1+(0.14/f_\mu)^3,$$

$$f_2 = [1-0.27\exp(-R_t^2)][1-\exp(-R_n)]$$

together with $k = \partial\varepsilon/\partial n = 0$ at walls.

This low Reynolds number model, which in parts is similar to the model of Jones and Launder [15] (JL) and the model of Lam and Bermhorst [16] (LB), was developed in refs. [9, 14] where the object was to develop a model which *may* have the possibility of predicting free flow low Reynolds number effects (i.e. which are not due to near-wall effects). This can be of importance in ventilated rooms [17], where the flow can relaminarize due to weak production of turbulence or due to stable stratification. The model is furthermore consistent in the near-wall behaviour of the ε equation and allows simulation of the decay of grid turbulence; the LB model meets neither of these requirements. It should also be noted that the model solves the equation for the *physical* isotropic dissipation. The JL model, however, uses

$$\tilde{\varepsilon} = \varepsilon - 2\nu\left(\frac{\partial\sqrt{k}}{\partial n}\right)^2$$

as the dissipation variable. Since, close to walls, the normal gradient of $\tilde{\varepsilon}$ is much larger than that of ε [18], the low Reynolds model used in the present work does not require as fine a grid near walls as does the JL model.

4. SECOND-ORDER CORRECTIONS OF THE k–ε MODEL

Buoyancy effects in turbulent flows enhance the non-isotropy of the turbulence. In stable stratified flows ($\partial t/\partial y > 0$; see Fig. 1), as in the present case, the vertical component of the turbulent fluctuations, v, is damped, and the horizontal ones are amplified. In unstable flows ($\partial t/\partial y < 0$) v is amplified and u and w are damped [1]. The k–ε model accounts for these effects to a certain degree: the buoyancy source terms in the k and ε equations, which are proportional to $\partial t/\partial y$ (see equation (2)), damp or amplify k and ε depending on the sign of $\partial t/\partial y$. However, the model cannot produce the physical *non-isotropic* effects by amplifying the turbulent fluctuation in one direction and damping the other ones, or vice versa. Reynolds stress turbulence models, either in differential (DSM) or algebraic (ASM) form, can account also for these non-isotropic effects. In this study, the interest is focused on the algebraic Reynolds stress model, which has the form [2]

$$\overline{u_i u_j} = \tfrac{2}{3}\delta_{ij}k + \frac{k}{\varepsilon}\frac{(1-c_2)(P_{ij}-\tfrac{2}{3}\delta_{ij}P)}{c_1+(P+G)/\varepsilon-1} + \frac{k}{\varepsilon}\frac{(1-c_3)(G_{ij}-\tfrac{2}{3}\delta_{ij}G)}{c_1+(P+G)/\varepsilon-1}. \quad (3)$$

Two drawbacks of the algebraic stress model are that it is computationally much more expensive than the k–ε model, and that it is much less stable which causes convergence problems [4, 5]. As buoyancy-driven flows themselves are numerically very unstable, and as it is usually very hard to obtain convergent solutions [8, 9, 19], it is clearly not advisable to incorporate turbulence models which further enhance the convergence problems.

In the present work a new model which is a hybrid of the k–ε model and the algebraic Reynolds stress model is developed which accounts for the non-isotropic turbulence due to buoyancy. Here the isothermal part of $\overline{u_i u_j}$ is taken from the k–ε model (equation (2)), while the non-isotropic part due to buoyancy is taken from ASM, i.e. the last term in equation (3). The total $\overline{u_i u_j}$ can be written as

$$\overline{u_i u_j} = (\overline{u_i u_j})_{k-\varepsilon} + (\overline{u_i u_j})_{\mathrm{ASM}} \quad (4a)$$

where

$$(\overline{u_i u_j})_{k-\varepsilon} = -\nu_t\left(\frac{\partial U_i}{\partial x_j}+\frac{\partial U_j}{\partial x_i}\right)+\tfrac{2}{3}\delta_{ij}k \quad (4b)$$

$$(\overline{u_i u_j})_{\mathrm{ASM}} = \frac{k}{\varepsilon}\frac{(1-c_3)(G_{ij}-\tfrac{2}{3}\delta_{ij}G)}{c_1+(P+G)/\varepsilon-1} \quad (4c)$$

$$G_{ij} = -\beta(g_i\overline{u_j\theta}+g_j\overline{u_i\theta}); \quad G = \tfrac{1}{2}G_{kk}. \quad (4d)$$

The constants c_1 and c_3 are given the values 1.8 and 0.6, respectively [20]. Using the eddy viscosity assumption for $\overline{v\theta}$ in equation (2) and noting that

$$g_1 = g_3 = 0; \quad g_2 = -g$$

the Reynolds stresses in equation (4c) can be written as

$$(\overline{u^2})_{\mathrm{ASM}} = (\overline{w^2})_{\mathrm{ASM}} = \tfrac{2}{3}C\frac{\partial t}{\partial y} \quad (5a)$$

$$(\overline{v^2})_{\mathrm{ASM}} = -\tfrac{4}{3}C\frac{\partial t}{\partial y} \quad (5b)$$

$$(\overline{uv})_{\mathrm{ASM}} = -C\frac{\partial t}{\partial x} \quad (5c)$$

where

$$C = \frac{k}{\varepsilon}\frac{(1-c_3)\nu_t\beta g\,\sigma_t}{c_1+(P+G)/\varepsilon-1}.$$

As can be seen from equation (5), a positive vertical temperature gradient ($\partial t/\partial y > 0$) decreases $\overline{v^2}$ and increases $\overline{u^2}$ and $\overline{w^2}$ as is physically required. For this to be true C must remain positive. As it was found in the calculations that the denominator in the expression for C in some regions (see Fig. 9(a)) became negative (because $G < 0$ and $|G|$ was large), $P+G$ in the denominator was replaced by P, i.e.

$$C = \frac{k}{\varepsilon}\frac{(1-c_3)\nu_t\beta g\,\sigma_t}{c_1+P/\varepsilon-1}. \quad (5d)$$

Test calculations were also carried out in which the denominator was replaced by c_1 assuming local equilibrium, which was used by Gibson and Launder [21] with good results. This change of denominator did not affect the predicted results very much, suggesting that the replacement of $P+G$ by P in equation (5d) is a good approximation.

It may be noted that the ASM corrections of the normal Reynolds stresses do not affect the turbulent kinetic energy, since their sum is zero, i.e. (see equation (5))

$$(\overline{u^2})_{\mathrm{ASM}}+(\overline{v^2})_{\mathrm{ASM}}+(\overline{w^2})_{\mathrm{ASM}} = 0.$$

The corrections in equation (5) merely *redistribute* the turbulent kinetic energy between the x-, y- and z-directions. The contribution $(\overline{u_i u_j})_{\mathrm{ASM}}$ to the total Reynolds stress in equation (4a) can be seen as a linear uncoupled ASM correction to the k–ε model.

The Reynolds stress $\overline{u_i u_j}$ in equations (4) and (5) is used in the momentum equations and in the expression for the generation term, P, in equation (2). Equations (4) and (5) can also be used in the diffusion terms in the k, ε and t equations by utilizing the generalized gradient diffusion hypothesis of Daly and Harlow [22], which has the form

$$\overline{u_i\phi} = -c_\phi\frac{k}{\varepsilon}\overline{u_i u_j}\frac{\partial\Phi}{\partial x_k} \quad (6)$$

where $\Phi = k$, ε or t. In the present work, equation (6) is used for the turbulent flux of heat, $\overline{u_i\theta}$, since this quantity is expected to be more important than the turbulent fluxes of k and ε. The individual heat fluxes for the temperature can, using equation (6), be written as

$$(\overline{u\theta})_{\mathrm{ASM}} = -c_\theta \frac{k}{\varepsilon}\left[(\overline{u^2})_{\mathrm{ASM}}\frac{\partial t}{\partial x} + (\overline{uv})_{\mathrm{ASM}}\frac{\partial t}{\partial y}\right] \quad (7a)$$

$$(\overline{v\theta})_{\mathrm{ASM}} = -c_\theta \frac{k}{\varepsilon}\left[(\overline{uv})_{\mathrm{ASM}}\frac{\partial t}{\partial x} + (\overline{v^2})_{\mathrm{ASM}}\frac{\partial t}{\partial y}\right] \quad (7b)$$

where the constant c_θ is taken as [23]

$$c_\theta = \tfrac{3}{2} f_\mu c_\mu/\sigma_t.$$

The total turbulent heat fluxes, which are included in the temperature equation, are calculated as in equation (4a), i.e. the sum of the isothermal part $(\overline{u_i\theta})_{k-\varepsilon}$, using the Boussinesq assumption in equation (2), and the buoyant part taken from equation (7).

The buoyancy destruction term (destruction rather than production since $\partial t/\partial y < 0$) G in equation (2) in the k and ε equations is modelled using the Boussinesq assumption, i.e. $\overline{v\theta} = (\overline{v\theta})_{k-\varepsilon}$. Inclusion of also $(\overline{v\theta})_{\mathrm{ASM}}$ in G, i.e. $\overline{v\theta} = (\overline{v\theta})_{k-\varepsilon} + (\overline{v\theta})_{\mathrm{ASM}}$, in equation (2) was tested, but no convergent solution at all could be obtained, probably because $(\overline{v\theta})_{\mathrm{ASM}}$ contributes *too much* to the total generation (it is much larger than $(\overline{v\theta})_{k-\varepsilon}$ close to the walls, see Fig. 8). As remarked by Ince and Launder [23] the turbulent heat fluxes, $\overline{u_i\theta}$, *themselves* appear in the buoyancy generation term, G, whereas the diffusion terms include the *gradients* of the heat fluxes; in the latter case the effect of $\overline{u_i\theta}$ is, thus, smaller.

It should be noted that the hybrid model aims to account only for *buoyancy* induced non-isotropic effects; in cases when isothermal non-isotropic effects are important (e.g. streamline curvature) the hybrid model cannot account for these effects in any more degree than the standard k–ε model.

The hybrid model presented above probably cannot model the turbulence as accurately as an algebraic Reynolds stress model. First, in the latter model the whole Reynolds stress—not only the part which is due to buoyancy—is modelled with an ASM. Second, even the buoyancy part of the Reynolds stress, $(\overline{u_iu_j})_{\mathrm{ASM}}$, is probably more accurately modelled with an ASM, since separate algebraic equations are used for the turbulent heat fluxes when G_{ij} in equation (4d) is calculated, whereas in the hybrid model, these are modelled using the Boussinesq assumption. It is, of course, possible to use the same equations for $\overline{u_i\theta}$ (in equation (4d)) in the hybrid model as in the algebraic Reynolds stress model, but this would mean that the model would lose much of its simplicity. The main advantages of the hybrid model are, in the author's view (as mentioned in Section 1), that it is comparatively simple, numerically cheap and stable (see Section 5.3), and that it does take into account the non-isotropy of the turbulence due to buoyancy.

4.1. *Flows with rotation*

Buoyancy affected flows represent a type of flow in which most of the non-isotropy of the turbulence is due to a special physical phenomenon (buoyancy in this case). The contribution to the Reynolds stress due to this phenomenon is in the present work modelled using a more sophisticated turbulence model (ASM), whereas the remaining part of the Reynolds stress is modelled using the k–ε model. There are other types of flow to which this concept is applicable. One example is a flow in which the turbulence is affected by Coriolis forces due to rotation. For this, isothermal, type of flow the form of the Reynolds stress is [24, 25]

$$\overline{u_iu_j} = \tfrac{2}{3}\delta_{ij}k + \frac{k}{\varepsilon}\frac{(1-c_2)(P_{ij}-\tfrac{2}{3}\delta_{ij}P)}{c_1+(P+G)/\varepsilon-1} + \frac{k}{\varepsilon}\frac{R_{ij}}{c_1+(P+G)/\varepsilon-1} \quad (8)$$

where

$$R_{ij} = -2\Omega_p(\varepsilon_{ipq}\overline{u_qu_j} + \varepsilon_{jpq}\overline{u_qu_i}).$$

Here, the second term in equation (8) can be used as $(\overline{u_iu_j})_{\mathrm{ASM}}$ in equation (4a), and the remaining part of the Reynolds stress can be taken from equation (4b). The Reynolds stresses in the expression of R_{ij} can be taken either from the Boussinesq assumption in equation (4b), or as the sum of the two parts in equation (4a); the latter is probably more accurate, but it results in more complex expressions for $(\overline{u_iu_j})_{\mathrm{ASM}}$.

5. RESULTS

In this section, the buoyancy-driven flow in the cavity in Fig. 1 is calculated using the two different low Reynolds number turbulent models presented in Sections 3 (k–ε model) and 4 (hybrid model). The CELS solver is used as described in Section 2, and the QUICK scheme was used in the U, V and t equations, whereas the hybrid upwind/central scheme was used in the k and ε equations.

The calculated results are compared with the experiments by Cheesewright *et al.* [6], who made laser Doppler measurements in an air cavity with Rayleigh number 4×10^{10} [7]. The flow in the present test case is recirculating which is important for evaluating the performance of the hybrid model. In a parabolic flow (boundary layer type of flow) the normal Reynolds stress does not appear (the V equation—y normal to the wall—is not solved, and $\partial\overline{u^2}/\partial x$ is negligible), and, hence the ASM corrections of the diffusive normal Reynolds stresses do not appear in the equations.

Detailed predicted results for this configuration using the k–ε model can be found in Davidson [9]; this case has also been numerically simulated by Ince and Launder [23]. The experiments suffer from two problems: there is a considerable heat loss through the side walls, and there is a small heat loss through the (well insulated) top wall. Near the top wall the flow is exposed to a positive vertical temperature gradient, which acts to reduce the turbulent kinetic energy (see equation (2)); this should cause relaminarization (which does occur near the bottom wall). Due to the small heat loss through the top wall, the temperature gradient is reduced, and the expected relaminarization

does not occur. This results in asymmetry of the flow in the experiments, and for this reason the comparison between calculations and experiments is concentrated to the mid-plane, where end effects should not be so large.

The heat loss through the side walls reduces the core temperature, which further increases the asymmetry of the flow in the experiments, i.e. the 'diagonal symmetry' is lost (the flow in the upper right part of the cavity should be similar—or identical when temperature effects on density and laminar viscosity are not taken into account—to that in the lower left part of the cavity).

A grid with 56×56 interior nodes is used, and it is generated using the equation

$$x_m = x_{\max}\left\{-0.5\tanh\left[\alpha\left(2\frac{m}{n}-1\right)\right]\Big/ \tanh(-\alpha)+0.5\right\} \quad (9)$$

with $\alpha = 3.5$, where x_m denotes the coordinate of line number m; the same formula was used for the y-lines.

It is important that the grid is sufficiently fine in the boundary layers at the vertical walls, where large gradients prevail. The grid generated using equation (9) gives two grid lines with constant x located inside $x^+ = 1$ at $y/H = 0.5$. Knowing that the second interior x-line is located inside $x^+ = 1$, equation (9) gives, e.g. $x_1^+ \simeq 20$. As the boundary layer grows along the vertical walls ($y/H > 0.5$ at the hot wall, and $y/H < 0.5$ at the cold wall), the number of grid lines located in the boundary layer will increase. It should also be pointed out that the present low Reynolds number model does not require as fine a grid near walls as, for example, does that of Jones and Launder [15] (see Section 3).

5.1. *Mean velocities and temperatures*

In Fig. 2 the velocity field is presented in the form of the velocity vector field. The flow consists of a large clockwise vortex, and it can be seen that there are two small clockwise vortices near the mid-plane $y/H = 0.5$. The calculated V-profiles are compared with experimental data in Fig. 3 (the V-profile at $y/H = 0.7$ for the hybrid model is included in order to facilitate interpretation of Figs. 6–9). It can be seen that the agreement between prediction and experiments is good in the left half of the cavity; there are some discrepancies in the core region, but both predicted profiles are probably within the bounds of experimental uncertainty. The discrepancy between the predicted profiles and the experimental profile, near the cold (right) wall, is due to the aforementioned incomplete relaminarization at the top wall in the experiments. It can also be seen that the predictions using the two different turbulence models are close to one another; the largest differences (up to 10%) appear in the peak values of the velocity close to the walls. The fact that the largest differences appear near the vertical walls is due to that the ASM corrections of the shear stress $(\overline{uv})_{\text{ASM}}$ are largest here (see Fig. 6). The maximum velocity close to the hot wall is in better agreement with experiments for the k–ε model than for the hybrid model, but this is probably because the damping functions in the low Reynolds number model have been tuned using the k–ε model.

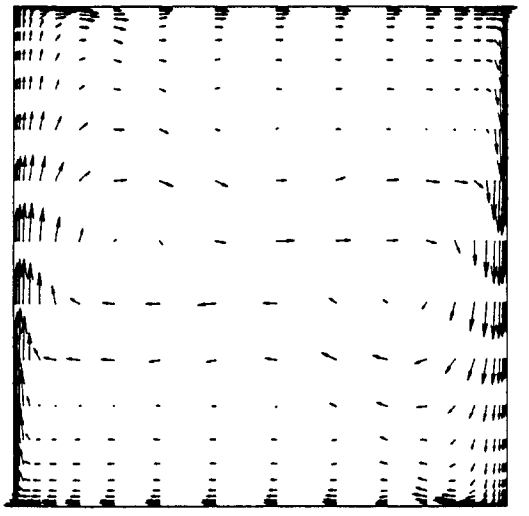

FIG. 2. Predicted velocity vector field. Hybrid model. Note change of scale in the x-direction (see Fig. 1).

Along the vertical walls Cheesewright *et al.* [6] presented the local Nusselt number as a function of the local Rayleigh number. A temperature difference, Δt, appears in the definitions of these two numbers, and in ref. [6] this temperature difference was taken as the difference between the hot wall and the local core temperature. Since the local core temperature is too low in the experiments, it was not considered relevant to compare predicted Nusselt number with the experimental one but it was considered preferable to compare the local heat transfer rates (in ref. [14] both comparisons can be found).

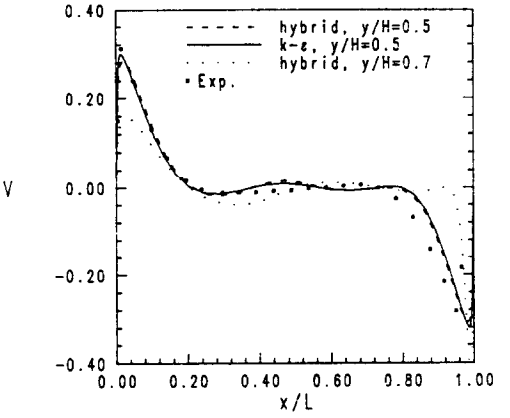

FIG. 3. Predicted and experimental V-velocity profiles at $y/H = 0.5$ and 0.7. Hybrid and k–ε model. Experiments at $y/H = 0.5$ by Cheesewright *et al.* [6].

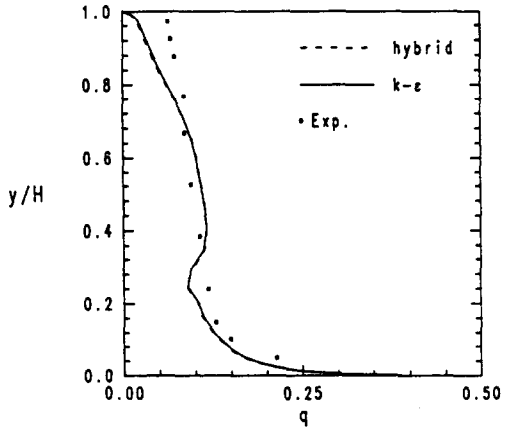

FIG. 4. Predicted and experimental local heat transfer rates at the left (hot) vertical wall. Hybrid and k–ε model. Experiments by Cheesewright *et al.* [6].

In Fig. 4 the predicted local heat transfer rate is compared with the experimental data along the hot (left) vertical wall. No comparisons are shown for the cold wall since the experimental data here are affected by the incomplete relaminarization at the top wall. It can be seen that the two turbulence models give almost the same heat transfer rate, with differences of less than 1% in the lower part ($y/H \leqslant 0.6$) of the hot wall.

The predictions exhibit a sharp increase of q at $y/H \simeq 0.25$, which shows that transition is predicted here. This is in rather good agreement with the experiments [6], where a transition region was found at approximately $y/H \simeq 0.2$.

5.2. *Turbulent quantities*

In Fig. 5 the predicted turbulent kinetic energy is compared with experimental data, and both turbulence models perform well. The hybrid turbulence model gives slightly higher maximum k-values, which are in better agreement with experiments, than the k–ε model. The turbulent shear stress, $\overline{uv}$, is shown in

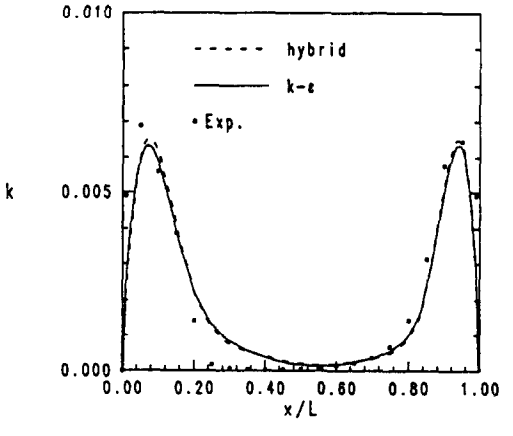

FIG. 5. Predicted and experimental turbulent energy, k, at $y/H = 0.5$. Hybrid and k–ε model. Experiments by Cheesewright *et al.* [6].

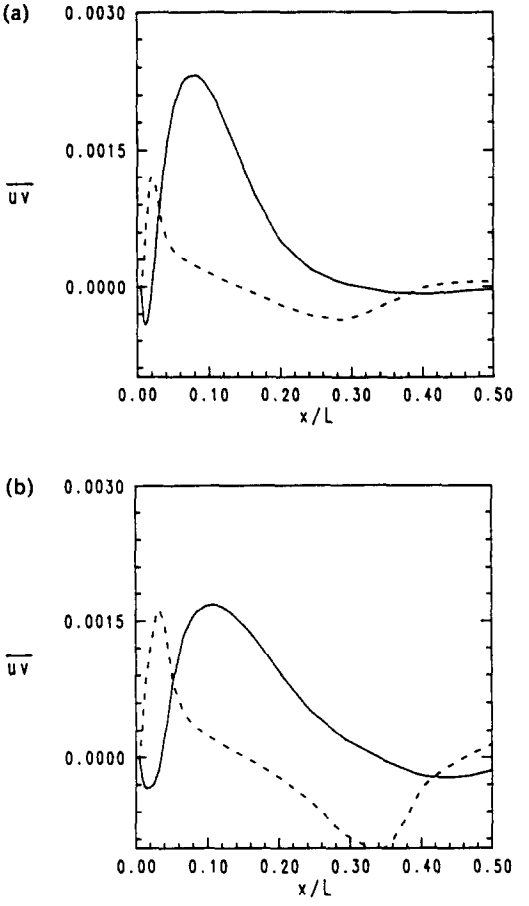

FIG. 6. Predictions obtained with the hybrid model. Predicted turbulent shear stress, $(\overline{uv})_{\text{ASM}}$ (– – –, equation (5c)) and $(\overline{uv})_{k-\varepsilon}$ (——, equation (4b)). (a) $y/H = 0.5$. (b) $y/H = 0.7$.

Fig. 6 at two different vertical levels. The isothermal part, $(\overline{uv})_{k-\varepsilon}$, and the buoyant part, $(\overline{uv})_{\text{ASM}}$, are presented separately. It can be seen that the buoyant part is dominant close to the wall. Since the velocity gradient $\partial V/\partial x$ is positive here $(\overline{uv})_{k-\varepsilon}$ is negative (see equation (4b)), and since the temperature gradient $\partial t/\partial x$ is negative, $(\overline{uv})_{\text{ASM}}$ is positive (see equation (5c)). The Reynolds stresses go to zero close to the wall because ν_t goes to zero.

The buoyant part of the Reynolds stress, $(\overline{uv})_{\text{ASM}}$, exhibits a dip at $x/L \simeq 0.34$, due to C in equation (5d) attaining its maximum values here. This is because the ratio k/ε increases as x increases and P/ε decreases from $x/L \simeq 0.1$ to 0.34, where P/ε starts to increase.

The normal Reynolds stress, $\overline{v^2}$, is presented in Fig. 7. Note that (see equation (5))

$$(\overline{u^2})_{\text{ASM}} = -\tfrac{1}{2}(\overline{v^2})_{\text{ASM}}.$$

In the mid-plane ($y/H = 0.5$) the buoyant part plays a negligible role compared with the isothermal part. At $y/H = 0.7$ $(\overline{v^2})_{\text{ASM}}$ is of the same size as $(\overline{v^2})_{k-\varepsilon}$ for $0.3 < x/L < 0.9$. The isothermal part of the normal Reynolds stress consists of two terms (see equation (4b)), namely $-2\nu_t \partial V/\partial y$ and $\frac{2}{3}k$ and it may be noted

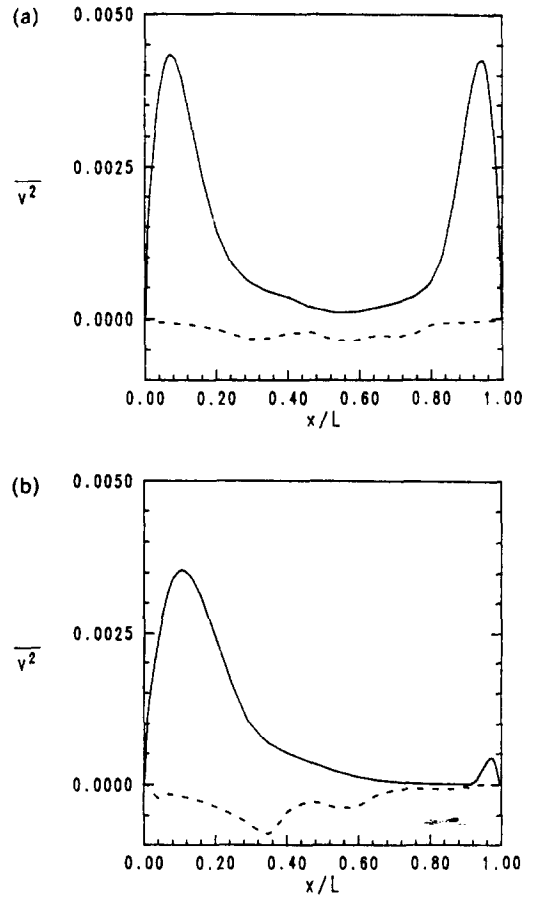

FIG. 7. Predictions obtained with the hybrid model. Predicted turbulent normal stress, $(\overline{v^2})_{ASM}$ (---, equation (5b)) and $(\overline{v^2})_{k-\varepsilon}$ (——, equation (4b)). (a) $y/H = 0.5$. (b) $y/H = 0.7$.

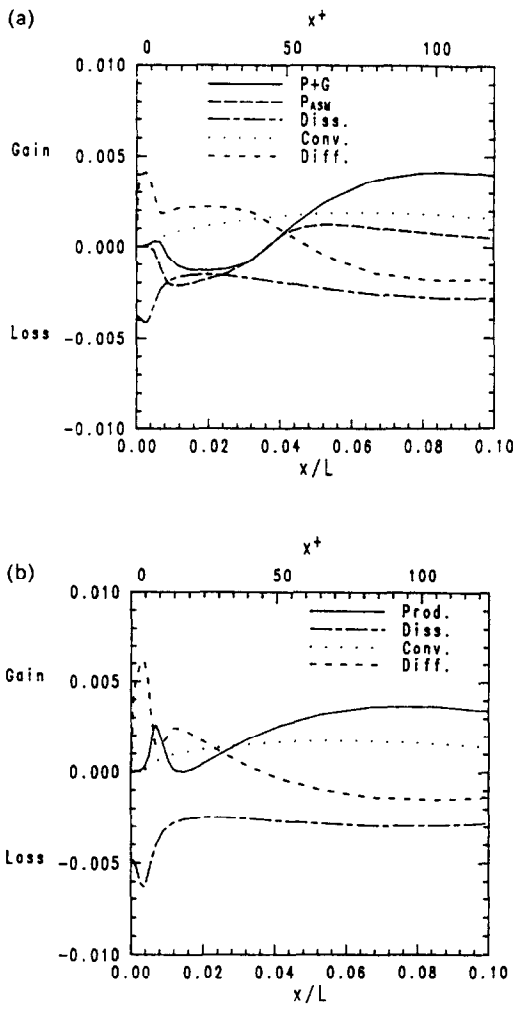

FIG. 9. Predicted turbulent kinetic budget at $y/H = 0.7$. Production, $P+G$; Production, $P_{ASM} = -(\overline{u_i u_j})_{ASM}\,\partial U_i/\partial x_j$; convection, $-\partial/\partial y(Vk)$; diffusion, $-\partial/\partial x[(\nu+\nu_t/\sigma_k)\partial k/\partial x]$; dissipation, $-\varepsilon$. (a) Hybrid model. (b) k–ε model.

that the first term is negligible compared with the second (cf. Figs. 5 and 7).

In Fig. 8 the turbulent heat flux $\overline{v\theta}$ is presented; $y/H = 0.7$ is chosen because the second-order corrections are larger here (see Fig. 6) than in the mid-plane. Close to the wall, the turbulent heat flux due to the ASM corrections is much larger than $(\overline{v\theta})_{k-\varepsilon}$. That $(\overline{v\theta})_{ASM}$ is large, close to the wall, was to be expected, since both $(\overline{uv})_{ASM}$ and $\partial t/\partial x$ here are large (see equation (7b) and Fig. 6). The turbulent heat flux $(\overline{v\theta})_{k-\varepsilon}$ is small because it is calculated using the vertical temperature gradient, $\partial t/\partial y$ (see equation (2)), which is significantly smaller than $\partial t/\partial x$. When the predicted turbulent heat flux due to the second-order corrections dominates over the isothermal one, why are the heat transfer rates predicted with the two turbulence models (see Fig. 4) so close to one another? The answer is that $\overline{v\theta}$ contributes to the vertical transport of heat. The turbulent diffusion which is responsible for the horizontal transport is small, since both terms in equation (7a) are small [$(\overline{u^2})_{ASM}$ and $\partial t/\partial y$ are small].

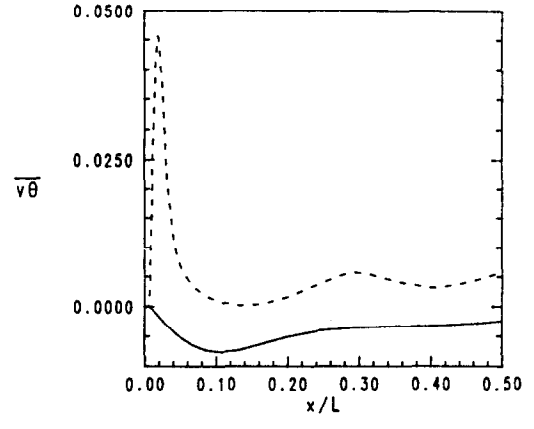

FIG. 8. Predictions obtained with the hybrid model. Predicted turbulent heat flux, $(\overline{v\theta})_{ASM}$ (---, equation (7b)) and $(\overline{v\theta})_{k-\varepsilon}$ (——, equation (2)). $y/H = 0.7$.

In order to further illustrate the effects of the ASM correction, the calculated turbulent kinetic energy budgets are shown for the hybrid model (Fig. 9(a)) and the k–ε model (Fig. 9(b)). It can be seen that, in the hybrid model, the generation term, $P+G$, is

significantly affected close to the wall. For $x^+ < 40$ the generation term due to the ASM corrections is negative and reduces the total generation so that it is even negative for $10 < x^+ < 40$. Consequently, the diffusion term in this region increases in order to balance the negative generation term and the dissipation term. The dissipation, ε, is smaller here than in Fig. 9(b), since the generation term is 'helping' ε to dissipate turbulent kinetic energy. Close to the wall at $x^+ \simeq 8$, the generation term predicted with the k–ε model has a peak which forces ε to increase in order to balance it, which, closer to the wall, results in larger dissipation and diffusion in Fig. 9(b) than in Fig. 9(a).

The main contribution to the generation term P_{ASM} is the shear stress term $(\overline{uv})_{ASM}\ \partial V/\partial x$. The shear stress is positive for $x/L < 0.16$ (see Fig. 6(b)), and the change of sign of the generation term P_{ASM} (at $x/L \approx 0.035$) is due to the change of sign of $\partial V/\partial x$ (see Fig. 3).

5.3. *Computational times*

The hybrid turbulence model requires only marginally more computational effort than the k–ε model. When using the low Reynolds k–ε model and the hybrid model the initial fields were taken from a calculation carried out using wall functions; this latter run required 1235 (false) time steps, and 4.8 h CPU time. Using these fields as initial fields the low Reynolds k–ε model required 2.4 h CPU and 585 time steps; the present model required 2.6 h CPU and 621 time steps. The present model thus requires 3% more in total CPU time than the k–ε model.

6. CONCLUSIONS

In some types of flow the non-isotropy of the turbulence is increased due to special physical phenomena, such as buoyancy and Coriolis forces. In the present work a turbulence model has been developed which is a hybrid of an algebraic Reynolds stress model and a k–ε model. In this model the part of the Reynolds stress which stems from buoyancy effects is modelled using an expression from an algebraic Reynolds stress model, while the remaining part is modelled using the k–ε model. The contribution of the algebraic Reynolds stress model to the Reynolds stress can be seen as a linear uncoupled correction to the k–ε model.

The main advantages of the hybrid model are that it is comparatively simple, numerically cheap and stable, and that it does take into account the non-isotropy of the turbulence due to buoyancy. It should be noted that the hybrid model aims to account only for *buoyancy* induced non-isotropic effects; in cases when isothermal non-isotropic effects are important (e.g. streamline curvature) the hybrid model cannot account for these effects in any more degree than the standard k–ε model.

The hybrid model and the k–ε model (in low Reynolds number form) have been tested in the buoyancy driven flow in a tall two-dimensional cavity of 5:1 aspect ratio. The CELS solver was used.

The following conclusions can be drawn:

(i) The new hybrid turbulence model can account for the non-isotropy due to buoyancy by—in stable, stratified flows—decreasing the vertical turbulent velocity fluctuation and increasing the horizontal ones, and vice versa in unstable flows.

(ii) The hybrid model requires only 3% more in CPU time than the k–ε model.

(iii) The contribution of the ASM corrections to the shear stress was, close to the vertical walls, up to five times larger (and of opposite sign) than the shear stress predicted by the k–ε model.

(iv) The vertical turbulent heat flux due to the ASM corrections was up to ten times larger than that predicted by the k–ε model. The horizontal flux, which is crucial for the prediction of the heat transfer rate at the vertical walls, was hardly affected by the ASM corrections.

(v) The ASM correction of the normal Reynolds stresses did not play a large role near the vertical walls, but the ASM corrections did significantly influence the normal stresses further away from the vertical walls.

This concept—adding corrections to the k–ε model to account for a particular physical phenomenon which increases the non-isotropy of the turbulence—should also be applicable for flows in which the turbulence is affected by Coriolis forces due to rotation. A suggestion for the expression of the Reynolds stress for this type of flow has been given in the present work.

In the present study the ASM correction in the new hybrid model has been shown to give corrections of turbulent quantities such as Reynolds stresses and turbulent heat fluxes qualitatively correct, but lack of experimental data prevents any quantitative estimation. Further validation of the model is thus needed.

Acknowledgements—The author is grateful to Prof. Lennart Löfdahl for his valuable comments. The Swedish Council for Building Research sponsored this work.

REFERENCES

1. H. Tennekes and J. L. Lumley, *A First Course in Turbulence*. MIT Press, Cambridge, Massachusetts (1972).
2. W. Rodi, Turbulence models and their application in hydraulics, International Association of Hydraulic Research, Monograph, Delft (1980).
3. M. Nallasamy, Turbulence models and their applications to the predictions of internal flows: a review, *Comput. Fluids* **15**, 151–194 (1987).
4. P. G. Huang and M. A. Leschziner, Stabilization of recirculating-flow computations performed with second-moment closures and third-order discretization, *Proc. 5th Int. Symp. on Turbulent Shear Flows*, pp. 20.7–20.12, Cornell (1985).
5. M. A. Leschziner, Numerical implementation and performance of Reynolds-stress closures in finite-volume computations of recirculating and strongly swirling

flows. Lecture notes to *Introduction to the Modelling of Turbulence*. von Karman Institute for Fluid Dynamics (1987).
6. R. Cheesewright, K. J. King and S. Ziai, Experimental data for the validation of computer codes for the prediction of two-dimensional buoyant cavity flows, *Significant Questions in Buoyancy Affected Enclosure or Cavity Flows*, Vol. HTD-60, pp. 75–81, ASME Winter Annual Meeting, Anaheim (1986).
7. R. Cheesewright, Private communication, Department of Mechanical Engineering, Queen Mary College, London (1988).
8. P. F. Galpin and G. D. Raithby, Numerical solution of problems in incompressible fluid flow: treatment of the temperature–velocity coupling, *Numer. Heat Transfer* **10**, 105–129 (1986).
9. L. Davidson, Calculation of the turbulent buoyancy-driven flow in a rectangular cavity using an efficient solver and two different low Reynolds number k–ε turbulence models, *Numer. Heat Transfer* **18**, 129–147 (1990).
10. P. F. Galpin and G. D. Raithby, Treatment of non-linearities in the numerical solution of the incompressible Navier–Stokes equations, *Int. J. Numer. Meth. Fluids* **6**, 409–426 (1986).
11. P. F. Galpin, J. P. Van Doormaal and G. D. Raithby, Solution of the incompressible mass and momentum equations by application of a coupled equation line solver, *Int. J. Numer. Meth. Fluids* **9**, 241–246 (1986).
12. J. P. Van Doormaal and G. D. Raithby, Enhancements of the SIMPLE method for predicting incompressible fluid flows, *Numer. Heat Transfer* **7**, 147–163 (1984).
13. B. P. Leonard, A stable and accurate convective modeling based on quadratic upstream interpolation, *Comp. Meth. Appl. Mech. Engng* **19**, 59–98 (1979).
14. L. Davidson, Numerical simulation of turbulent flow in ventilated rooms, Ph.D. thesis, Dept. of Applied Thermodynamics and Fluid Mechanics, Chalmers University of Technology, Göteborg (1989).
15. W. P. Jones and B. E. Launder, The prediction of laminarization with a two-equation model of turbulence, *Int. J. Heat Mass Transfer* **15**, 301–314 (1972).
16. C. K. G. Lam and K. A. Bremhorst, A modified form of the k–ε model for predicting wall turbulence, *J. Fluid Engng* **103**, 456–460 (1981).
17. L. Davidson, Ventilation by displacement in a three-dimensional room: a numerical study, *Bldg Envir.* **24**, 363–372 (1989).
18. V. C. Patel, W. Rodi and G. Scheurer, Turbulence models for near-wall and low Reynolds number flows: a review, *AIAA J.* **23**, 1308–1319 (1986).
19. I. P. Jones, The convergence of a simple iterative strategy for strongly stratified flows, *Proc. 4th Int. Conf. on Numer. Meth. in Laminar and Turbulent Flow*, Swansea, Vol. 1, pp. 733–740 (1985).
20. M. Ljuboja and W. Rodi, Prediction of horizontal and vertical turbulent buoyant wall jets, *ASME Fluids Engng* **103**, 343–349 (1981).
21. M. M. Gibson and B. E. Launder, Ground effects on pressure fluctuations in the atmospheric boundary layer, *J. Fluid Mech.* **86**, 491–512 (1978).
22. B. J. Daly and F. H. Harlow, Transport equations of turbulence, *Physics Fluids* **13**, 2634–2649 (1970).
23. N. Z. Ince and B. E. Launder, Computation of turbulent natural convection in closed rectangular cavities, *Proc. 2nd U.K. Natn. Conf. on Heat Transfer*, University of Strathclyde, Glasgow, Vol. 2, pp. 1389–1400 (1988).
24. H. Iacovides and B. E. Launder, The numerical simulation of flow and heat transfer in tubes in orthogonal-mode rotation, *Proc. 6th Int. Symp. on Turbulent Shear Flows*, pp. 1.5.1–1.5.6, Toulouse (1987).
25. J. M. Galmes and B. Lakshminarayana, Turbulence modeling for three-dimensional shear flows over curved rotating bodies, *AIAA J.* **22**, 1420–1428 (1984).

CORRECTIONS DE SECOND ORDRE DU MODELE k–ε POUR TENIR COMPTE DES EFFETS NON ISOTROPES DE LA PESANTEUR

Résumé—On développe un nouveau modèle de turbulence hybride entre le modèle k–ε et un modèle algébrique de tension de Reynolds (ASM). Ce modèle tire de l'ASM la prise en compte des tensions de Reynolds non isotropes dues à la pesanteur et du modèle k–ε ses avantages propres. Ce concept est applicable aussi aux écoulements avec rotation où les forces de Coriolis affectent la turbulence en augmentant le défaut d'isotropie. Ce modèle est testé avec un écoulement avec flottement dans une cavité. Les contributions des corrections dues à l'ASM sur les contraintes de Reynolds et les flux thermiques turbulents sont respectivement jusqu'à cinq et dix fois plus grands que ce que donnerait le modèle k–ε.

KORREKTUREN ZWEITER ORDNUNG IM k–ε-MODELL ZUR BERÜCKSICHTIGUNG AUFTRIEBSBEDINGTER ANISOTROPIE

Zusammenfassung—Es wird ein neues Turbulenzmodell entwickelt, das sich aus dem k–ε-Modell und einem algebraischen Modell für die Reynolds'schen Schubspannungen (ASM) zusammensetzt. Dieses Modell übernimmt aus dem ASM den auftriebsbedingten Teil der nicht-isotropischen Reynolds'schen Schubspannungen—den Rest aus dem k–ε-Modell. Dieses Konzept kann ebenso auf Rotationsströmungen angewandt werden, bei denen die Coriolis-Kräfte durch zunehmende Anisotropie den Turbulenzgrad beeinflussen. Das Modell wird anhand einer Auftriebsströmung in einem Hohlraum getestet. Die Beiträge der ASM-Korrekturglieder zu den Reynolds'schen Schubspannungen und zum turbulenten Wärmestrom sind bis zu 5mal und 10mal größer als diejenigen vom k–ε-Modell.

ПОПРАВКИ ВТОРОГО ПОРЯДКА МОДЕЛИ k–ε ДЛЯ УЧЕТА НЕИЗОТРОПНЫХ ЭФФЕКТОВ, ВЫЗВАННЫХ ПОДЪЕМНЫМИ СИЛАМИ

Аннотация—Разработана новая модель турбулентности, сочетающая модель k–ε и алгебраическую модель рейнольдсовского напряжения (ASM). В этой модели частично используются неизотропное рейнольдсовское напряжение из алгебраической модели, обусловленное подъемными силами, и из модели k–ε. Данное понятие также применимо к течениям с закруткой, где воздействие кориолисовых сил на турбулентность заключается в увеличении ее неизотропности. Модель проверена на кавитационном течении, вызванном подъемными силами. Оказалось, что вклад от поправок к рейнольдсовским напряжениям и тепловому потоку, связанный с алгебраической моделью, соответственно в пять и десять раз больше, чем вклад, связанный с k–ε моделью.